

Inhomogeneous magnetism in La-doped CaMnO_3 . (I) Nanometric-scale spin clusters and long-range spin canting

E. Granado,^{1,2,3} C. D. Ling,^{4,5} J. J. Neumeier,⁶ J. W. Lynn,^{1,2} and D. N. Argyriou⁵

¹*NIST Center for Neutron Research, National Institute of Standards and Technology, Gaithersburg, Maryland 20899*

²*Center for Superconductivity Research, University of Maryland, College Park, Maryland 20742*

³*Laboratório Nacional de Luz Síncrotron, Caixa Postal 6192, CEP 13084-971, Campinas, SP, Brazil*

⁴*Institut Laue-Langevin, BP 156, 38042 Grenoble Cedex 9, France*

⁵*Materials Science Division, Argonne National Laboratory, Argonne, Illinois 60439*

⁶*Department of Physics, Montana State University, Bozeman, MT 59717*

Neutron measurements on $\text{Ca}_{1-x}\text{La}_x\text{MnO}_3$ ($0.00 \leq x \leq 0.20$) reveal the development of a liquid-like spatial distribution of magnetic droplets of average size ~ 10 Å, the concentration of which is proportional to x (one cluster per ~ 60 doped electrons). In addition, a long-range ordered ferromagnetic component is observed for $0.05 \lesssim x \lesssim 0.14$. This component is perpendicularly coupled to the simple G -type antiferromagnetic (G -AFM) structure of the undoped compound, which is a signature of a G -AFM+FM spin-canted state. The possible relationship between cluster formation and the stabilization of a long-range spin-canting for intermediate doping is discussed.

PACS numbers: 61.12.-q; 75.25.+z; 61.25.-f; 75.60.-d

I. INTRODUCTION

Doped manganites are strongly correlated electron systems with unusually large responses to external perturbations such as magnetic field and pressure. While the most dramatic effects such as colossal magnetoresistance have been observed in heavily-doped compounds, systematic studies on lightly and moderately-doped samples may reveal some fundamental aspects of manganite physics. In these regimes, the antiferromagnetic (AFM) spin structures shown by the undoped compounds tend to be destabilized by the ferromagnetic (FM) exchange interactions mediated through the charge carriers. Electron-doped CaMnO_3 samples are particularly attractive model systems due to the relative simplicity and chemical stability of the parent compound, which shows a simple quasi-cubic crystal structure and an isotropic G -AFM spin ground state¹. For electron-doped CaMnO_3 , a relatively weak ferromagnetism has been observed up to ~ 15 % doping^{2,3,4,5,6}. While the classic de Gennes theory for lightly-doped manganites describes the weak ferromagnetism in terms of spin-canted ground states⁷, a number of more recent theoretical studies indicate that homogeneous canted magnetic structures may not be energetically stable, suggesting a tendency towards magnetic and electronic phase segregation for both hole-doped^{8,9,10,11,12,13,14,15,16,17} and electron-doped^{14,15,16,17,18} manganites. In fact, for moderately hole-doped LaMnO_3 (5 – 8 % Ca- or Sr- doping), single crystal neutron-scattering studies revealed the existence of nanometric-scale magnetic inhomogeneities at low T ^{19,20,21}. Whether electron-doped manganites actually mirror this effect is an open experimental problem and a fundamental issue, since the phase diagram of electron-doped manganites is in general asymmetrical with respect to their hole-doped counterparts. For instance, the ferromagnetic metallic ground state is not re-

alized for La-doped CaMnO_3 , in stark contrast with the wide compositional interval where this state is observed in Ca-doped LaMnO_3 .

Previous dc-magnetization^{5,23}, thermal conductivity²³, Raman-scattering²⁴, and electron spin resonance²⁴ studies on $\text{Ca}_{1-x}\text{La}_x\text{MnO}_3$ indicate a crossover between distinct doping regimes at $x \sim 0.03$, which in this paper we refer to as low-doping ($0 < x \lesssim 0.03$) and intermediate-doping ($0.03 \lesssim x \lesssim 0.15$) regimes. While it has been suggested that this crossover may reflect novel polaron physics²³, not much direct information on the microscopic structure of the weak ferromagnetism observed for electron-doped manganites is presently available. A notable exception is an NMR study performed on $\text{Ca}_{1-x}\text{Pr}_x\text{MnO}_3$ ($x \leq 0.1$)²⁵, which found a coexistence of ferromagnetism and antiferromagnetism in the samples studied, thus supporting a phase segregation scenario.

In this work, the microscopic structure of the magnetic ground states of ceramic pellets of $\text{Ca}_{1-x}\text{La}_x\text{MnO}_3$ ($x = 0.00, 0.02, 0.03, 0.05, 0.06, 0.07, 0.09, 0.12, 0.16, \text{ and } 0.20$) are investigated by neutron measurements. We focus on the compounds with $x = 0.02$ and $x = 0.09$, which are representative members of the low- and intermediate-doping regimes, respectively. Elastic scattering at low angles reveals a liquid-like spatial distribution of magnetic clusters of average size ~ 10 Å in both regimes, whose concentration in the G -AFM matrix is proportional to the doping level. Diffraction measurements under applied magnetic fields reveal that the G -AFM and FM spin components are uncoupled for low-doping and become orthogonally coupled as the doping increases. Such orthogonal coupling is a signature of a spin-canted state. Small-angle neutron scattering (SANS) measurements also show magnetic domain-wall scattering in the intermediate doping regime, revealing a long-range FM component. The combined results severely limit the possible scenarios for the development of the FM moment

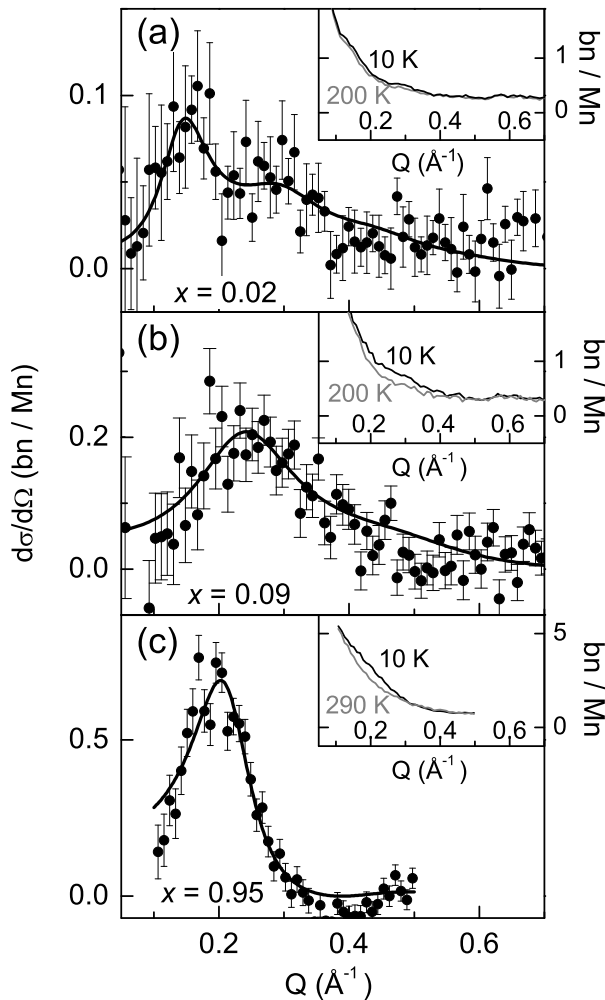


FIG. 1: Elastic magnetic cross section versus Q for $\text{Ca}_{1-x}\text{La}_x\text{MnO}_3$ for $x = 0.02$ (a), $x = 0.09$ (b), and $x = 0.95$ (c). The solid lines are fits to a liquid-like distribution model of magnetic droplets (see text). The insets show the raw data at 10 K and 200 K (290 K for $x = 0.95$).

in electron-doped manganites. In fact, they indicate a non-trivial magnetism for this system, which cannot be described either by a homogeneously spin-canted state⁷, or by a radical phase segregation where FM clusters are embedded into a pure G -AFM matrix.

II. RESULTS AND ANALYSIS

The La-doped CaMnO_3 samples were prepared by standard solid state reaction, as described in detail in the following paper.²⁶ A hole-doped sample, $\text{Ca}_{0.05}\text{La}_{0.95}\text{MnO}_3$, was prepared in a similar manner to the other samples, but was reacted in Argon at all stages of the preparation and reacted to a maximum temper-

ature of 1250 °C to keep the defect concentration low. Elastic neutron scattering experiments at low angles were performed using the BT-2 triple-axis spectrometer at the NIST Center for Neutron Research, with $E = 14.7$ meV and $(60' - 20' - 20' - 80')$ collimation. The insets of Figs. 1(a) and 1(b) show the elastic scattering at 10 K and 200 K for $\text{Ca}_{1-x}\text{La}_x\text{MnO}_3$ with $x = 0.02$ and 0.09 , in the Q -interval between 0.05 \AA^{-1} and 0.7 \AA^{-1} . The elastic magnetic scattering at low- T ($I_M(Q)$) can be more readily identified by subtracting the elastic scattering at 200 K from the intensities at 10 K. This is shown in Figs. 1(a) and 1(b) (symbols). The solid lines are fits to a liquid-like model for the spatial distribution of similar rigid magnetic droplets^{20,21,27}. The full expression for $I_M(Q)$ under this model is given in ref.²⁰. The shape of $I_M(Q)$ is determined by the minimum distance between clusters (d_{min}), droplet diameter (D), and cluster concentration (N_V). For $x = 0.02$, the fitting parameters are $d_{min} = 41(3) \text{ \AA}$, $N_V = 6.6(1.4) \cdot 10^{-6} \text{ \AA}^{-3}$ (i.e., one droplet per $\sim 59(12)$ doping electrons), and $D = 10.4(1.8) \text{ \AA}$. For $x = 0.09$, we obtain $d_{min} = 24(2) \text{ \AA}$, $N_V = 28(6) \cdot 10^{-6} \text{ \AA}^{-3}$ (1 cluster per 63(14) doping electrons), and $D = 10.6(1.6) \text{ \AA}$ (see footnote²⁸). Errors given in parentheses are statistical only and represent one standard deviation. We note that fits to $I_M(Q)$ of Fig. 1 assuming clusters with soft walls were also performed, providing equally good fits to the experimental data and nearly identical results for N_V and d_{min} . In fact, the calculated profiles shown in Figs. 1(a) and 1(b) are mostly determined by inter-cluster diffraction, except for the overall intensity decay at $Q \gtrsim 0.4 \text{ \AA}^{-1}$ due to the finite cluster size. Thus, little information on the cluster shape and rigidity can be directly obtained from this experiment. Elastic scattering experiments were also performed at 10 K and 290 K for a polycrystalline hole-doped manganite, $\text{Ca}_{0.05}\text{La}_{0.95}\text{MnO}_3$ (see Fig. 1(c)). The subtracted intensity, $I(10 \text{ K}) - I(290 \text{ K})$, shows a peak at $Q \sim 0.2 \text{ \AA}^{-1}$, for which the intensity, shape and width are in good agreement with previously published results for a single crystal of the same compound²¹. This indicates that the magnetic clusters observed for lightly hole-doped manganites^{20,21} are essentially insensitive to the sample growth method. This result, combined with the evidence for magnetic clusters reported here for electron-doped manganites, supports a universal tendency for intrinsic inhomogeneous ground states in lightly-doped manganites.

The possibility of a long-range FM component was investigated by energy-integrated SANS. The FM scattering peaks at $Q = 0$, and shows a distribution in the Q -scale of $\sim 2\pi/L_d$, where L_d is the average domain size. The experiments were performed using the NG-1 instrument at NIST, with $\lambda = 12 \text{ \AA}$, and a sample-detector distance of 3.5 m. The intensities were measured by a two-dimensional position-sensitive detector ($0.007 \text{ \AA}^{-1} < Q < 0.08 \text{ \AA}^{-1}$), and were angularly averaged around the beam-center position. Figure 2(a) shows $I(Q)$ at 10 K and 200 K for $x = 0.09$. Although the SANS

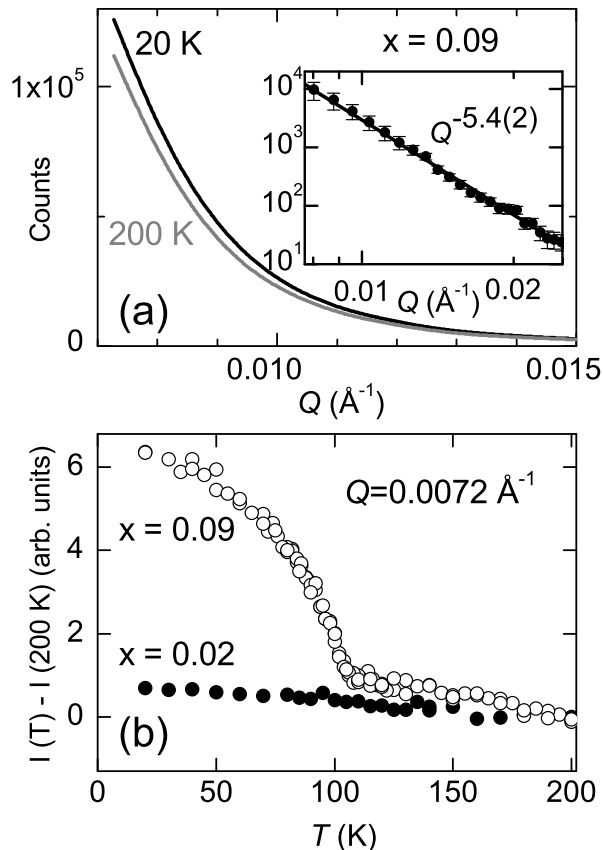


FIG. 2: (a) SANS for $\text{Ca}_{1-x}\text{La}_x\text{MnO}_3$ at 20 K and 200 K for $x = 0.09$. The inset shows $I(20\text{ K}) - I(200\text{ K})$ and a fit to a power law. (b) T -dependence of the scattering at $Q = 0.0072\text{ \AA}^{-1}$ for $x = 0.02$ and $x = 0.09$. Data in (b) were corrected for thickness and absorption to allow a direct comparison between samples.

data are dominated by a non-magnetic and slightly T -dependent component (most likely from intergrain scattering), a magnetic component is also clearly present for $x \geq 0.05$. This is evidenced by the T -dependence of the scattering at $Q = 0.0072\text{ \AA}^{-1}$, showing a significant enhancement below T_C ($= 108(1)\text{ K}$ for $x = 0.09$, see Fig. 2(b)). The inset of Fig. 2(a) shows the intensities at 10 K after subtracting the background scattering at 200 K, and a fit to a power-law behavior, $I = A Q^{-5.4(2)}$, for Q between 0.007 \AA^{-1} and 0.025 \AA^{-1} . This result indicates the existence of magnetic domains with sizes of several hundred Angstroms or larger, evidencing a long-range FM component. This conclusion is also supported by polarization-dependent neutron diffraction of a nuclear Bragg peak for $x = 0.09$, which showed the neutron beam being depolarized by the sample below T_C (not shown). For $x = 0.02$, no evidence for domain-wall scattering was observed by SANS, within our experimental sensitivity (see Fig. 2(b)).

Powder diffraction experiments were carried out over an extended Q -range²⁶. For $x = 0.02$ and 0.03 , G -AFM Bragg peaks were observed at low T ; the weak FM component seen by dc-magnetization⁵ was below our experimental sensitivity. For $0.06 \leq x \leq 0.12$, G -AFM Bragg peaks and FM intensities on top of nuclear Bragg peaks were observed at low- T , as well as magnetic reflections from the C -type AFM structure (C -AFM)¹. The FM Bragg intensities confirm the existence of a spontaneous long-range FM component in the intermediate-doping regime, in accordance with our SANS measurements (see above). For $x = 0.16$ and 0.20 , only C -AFM magnetic Bragg peaks were observed. A combined analysis using high-resolution neutron and synchrotron X-ray diffraction data makes it clear that the C -AFM magnetic reflections originate in crystallographic domains having a distinct (monoclinic) crystal structure due to the elongation of MnO_6 octahedra along the C -AFM chain direction. Such regions coexist on a mesoscopic scale with orthorhombic domains possessing regular MnO_6 octahedra. Details are given in the following paper.²⁶

To clarify the microscopic relationship between the FM signal and the G -AFM and C -AFM spin components, H -dependent neutron diffraction experiments were carried out on BT-2 with $E_i = E_f = 14.7\text{ meV}$ and $(60' - 40' - 40' - \text{open})$ collimation. The field was applied perpendicularly to the plane defined by the incident and scattered wave vectors, using a superconducting magnet. The magnetic intensities are proportional to the square of the sublattice magnetization, and also to the geometrical factor $\gamma \equiv \langle 1 - (\widehat{\mathbf{M}} \cdot \widehat{\boldsymbol{\tau}})^2 \rangle$, where $\widehat{\boldsymbol{\tau}}$ and $\widehat{\mathbf{M}}$ are the directions of the reciprocal lattice vector and the sublattice magnetization, respectively, and the brackets account for a domain-average. For cubic or quasi-cubic crystal lattices, $\gamma(\mathbf{H} = 0) = 2/3$. Under the application of \mathbf{H} , the FM component reorients along the field direction. Therefore, for increasing $\mathbf{H} \perp \widehat{\boldsymbol{\tau}}$, such as in our experiment, one has $\gamma_{FM}(\mathbf{H}) \rightarrow 1$. The coupling of the AFM to the FM moments can be inferred from the \mathbf{H} -dependence of γ_{AFM} , as described below (see also refs.¹ and²⁹).

Figure 3(b) shows the field-dependence of the $(1, 0, 0)$ nuclear + FM, $(\frac{1}{2}, \frac{1}{2}, \frac{1}{2})$ G -AFM, and $(\frac{1}{2}, \frac{1}{2}, 0)$ C -AFM Bragg peaks (cubic notation) for $x = 0.09$. The inset of Fig. 3(b) shows in detail the peak intensity of the $(1, 0, 0)$ reflection. The observed increase of this peak intensity for increasing fields up to $\sim 0.5\text{ T}$ indicates a reorientation of the FM spin-component along the field direction (see above). The intensity of the $(\frac{1}{2}, \frac{1}{2}, \frac{1}{2})$ peak decreases by $34(3)\%$ in the same field range, indicating a perpendicular coupling between G -AFM and FM spin components, consistent with G -AFM + FM spin-canting. The intensity of the $(\frac{1}{2}, \frac{1}{2}, 0)$ peak is insensitive to fields up to 7 T , showing that the C -AFM spin component is not coupled to the FM spin component. Thus, the results shown in Fig. 3(b), combined with high-resolution diffraction data²⁶, suggest mesoscopic phase coexistence between C -AFM regions with no FM moment and G -AFM + FM state for $0.06 \lesssim x \lesssim 0.12$.

III. DISCUSSION

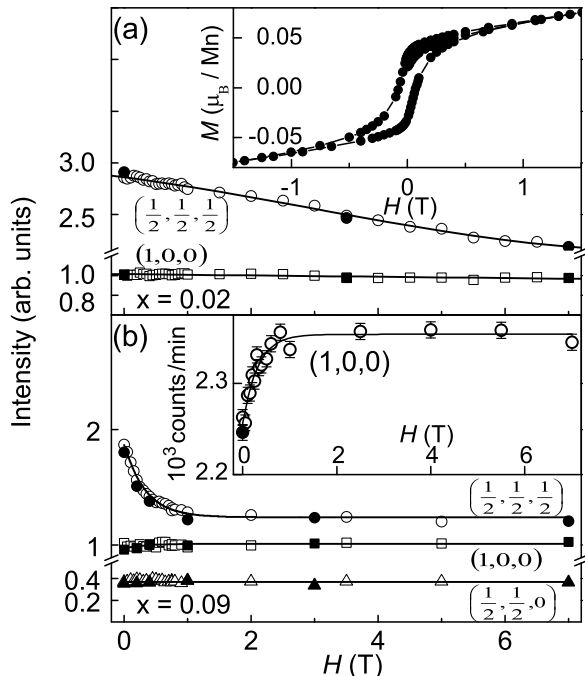


FIG. 3: H -dependence at 5 K of the intensity of the $(\frac{1}{2}, \frac{1}{2}, \frac{1}{2})$ G -AFM and $(1, 0, 0)$ nuclear + FM Bragg reflections for $x = 0.02$ (a) and $x = 0.09$ (b), and $(\frac{1}{2}, \frac{1}{2}, 0)$ C -AFM reflection for $x = 0.09$. Empty (filled) symbols represent increasing (decreasing) fields. The insets show the H -dependence at 5 K of the dc-magnetization for $x = 0.02$ and of the peak intensity of the $(1, 0, 0)$ Bragg reflection for $x = 0.09$.

For $x = 0.02$, the field-induced reorientation of the very weak FM spin component was probed by dc-magnetization (M_{dc}) measurements, which were taken using a commercial SQUID magnetometer. The inset of Fig. 3(a) shows the H -dependence of M_{dc} at 5 K. The curve can be decomposed into a FM signal which saturates at $\sim 0.05\mu_B/\text{Mn}$ for fields smaller than 0.5 T, and a linear component which is tentatively ascribed to a conventional field-induced spin canting. The field-dependence of the G -AFM spins for $x = 0.02$ was probed by neutron diffraction (see Fig. 3(a)). An intensity decrease of the $(\frac{1}{2}, \frac{1}{2}, \frac{1}{2})$ reflection was observed in the field scale of several tesla. This effect is not directly connected to the reorientation of the spontaneous FM moments, which takes place for $H < 0.5$ T (see inset of Fig. 3(a)). Thus, for $x = 0.02$, the G -AFM moments are not coupled to the FM moments, at least for small fields ($H < 0.5$ T), and the origin of the weak FM signal for this compound is inconsistent with a zero-field spin-canting of the G -AFM structure.

The observation of magnetic clusters (see Fig. 1) clearly points to a spatially inhomogeneous charge-carrier distribution in this system. The ratio between doped electrons and cluster densities (~ 60 , see above) is independent of x for electron-doped manganites and is identical to that found in hole-doped manganites^{20,21}, strongly suggesting a universal behavior. However, this large ratio and the small dimensions of the observed clusters (comprising ~ 10 unit cells) make it clear that only a fraction of the doped electrons are inside such clusters. The correct mechanism that leads to this phenomenon is not clear at this point. Even with a few electrons in each cluster, the charge contrast inside and outside the droplets may be exceedingly high, particularly in the low-doping regime. Simple electrostatic considerations indicate that the Coulomb energy loss for a FM two-electron droplet with $D \sim 10$ Å surrounding a La^{3+} ion is of the order of 1 eV for low- and intermediate-doping regimes, and increases quadratically with the number of cluster electrons. This Coulomb energy might overwhelm the delocalization energy gain per electron in the cluster ($t \sim 0.1 - 1$ eV), as already pointed out by Chen and Allen³⁰. In this context, it would appear natural to consider that clusters might be formed by electrostatic attraction in La-rich regions of the sample, presumably associated with intrinsic chemical inhomogeneities³¹. This mechanism would lead to electrically-neutral, Mn^{3+} -rich, magnetic clusters. The relatively small cluster densities would be naturally accounted for in this scenario. On the other hand, the cluster diffraction profiles shown in Figs. 1(a) and 1(b) imply a spatial short-range order similar to a liquid state, as opposed to a cluster gas where the cluster positions would be uncorrelated. Such an order suggests intercluster repulsion, presumably dictated by Coulomb forces between electrically charged and mobile clusters. The cluster diffraction also implies that neighboring clusters are magnetically correlated in both low- and intermediate-doping regimes, as opposed to a superparamagnetic state. In view of the above considerations, we believe that a truly intrinsic mechanism for small cluster formation in this system, i.e., not caused by chemical inhomogeneities, should not be discarded at this point.

The electrons outside the small magnetic clusters discussed above are likely to be important for the overall magnetic behavior of La-doped CaMnO_3 . In fact, using the fitting parameters obtained from Fig. 1, the total cluster contributions to the sample-average magnetizations are estimated to be $0.02(1)\mu_B/\text{Mn}$ for $x = 0.02$ and $0.04(2)\mu_B/\text{Mn}$ for $x = 0.09$, which are significantly smaller than the saturation magnetizations obtained from dc-magnetometry, 0.05 and $0.40\mu_B/\text{Mn}$, respectively⁵. Also, the combination of a long-range FM spin component and the orthogonal coupling between FM and G -AFM spin components at intermediate-doping is a signature of a long-range G -AFM + FM spin-canted state that does not appear to be accomplished at the

low-doping regime. Although the present set of experimental data, combined with previous work on La-doped CaMnO_3 ^{4,5,23,24}, may be insufficient to lead to a complete description for the microscopic structure of the FM moments and doped electrons in this system, it severely constrains any plausible model, as described below.

It is clear from the results above that a second type of doped electron is present in La-doped CaMnO_3 , besides the type forming relatively small FM clusters ($D \sim 10$ Å). Given the long-range spin-canted state evidenced for intermediate doping, the extra electrons seem to be delocalized on the atomic scale. On the other hand, the fact that a metallic state is not accomplished at low temperatures⁴, combined with the absence of an observable long-range FM component at low-doping, suggests that such extra electrons are not fully delocalized into a de Gennes canted state⁷ either. Thus, we suggest that these electrons are segregated into spin-canted regions of finite size, presumably larger than the small FM clusters directly observed by neutrons. These regions would overlap for intermediate-doping, leading to the observed long-range FM component perpendicularly coupled to the G -AFM moments. We note that such hypothetical spin-canted clusters were not directly observed in our neutron scattering measurements, possibly due to the small magnetization contrast and/or large sizes leading to small differential cross section in the Q -region accessible for elastic measurements (see Fig. 1). From a theoretical point of view, the formation of an inhomogeneous G -AFM+FM spin-canted state in electron-doped manganites, evidenced in this work, might be the result of a balance between the well-known electronic instability of the homogeneous spin-canted G -AFM state^{14,15,16,17,18} and the large Coulomb energy cost of a radical phase seg-

regation scenario where purely FM droplets are formed into a pure G -AFM background.

IV. CONCLUSIONS

Our results on La-doped CaMnO_3 indicate that a fraction of the doped electrons segregate into small ($D \sim 10$ Å) FM clusters embedded in the G -AFM matrix of the undoped compound. The remaining electrons are presumably delocalized over a more extended volume, leading to an inhomogeneous spin-canted state at intermediate doping. The density of the 10 Å-clusters, as well as the FM component of the spin-canted state, increase with the doping level, and the overall FM moment becomes increasingly dominant over the G -AFM spin component. Nevertheless, the pure FM metallic state is never stabilized for La-doped CaMnO_3 , due to the gradual emergence of the orbitally-ordered C -AFM state for $x \gtrsim 0.06$, which competes with the G -AFM + FM state through a first-order phase transition, as explored in the following paper²⁶. This competition leads to mesoscopic magnetic and crystallographic phase separation over a large x - and T -interval, and finally to the stabilization of the C -AFM phase for $0.16 \lesssim x \lesssim 0.20$ ^{26,32,33,34}.

V. ACKNOWLEDGEMENTS

This work was supported by FAPESP, Brazil, NSF-MRSEC, DMR 0080008, NSF DMR 9982834, and US Department of Energy, Basic Energy Sciences - Materials Sciences, contract W-31-109-ENG-38, USA.

-
- ¹ E.O. Wollan and W.C. Koehler, Phys. Rev. **100**, 545 (1955).
² H. Chiba, M. Kikuchi, K. Kusaba, Y. Muraoka, and Y. Syono, Solid State Commun. **99**, 499 (1996).
³ A. Maignan, C. Martin, F. Damay, and B. Raveau, Chem. Mater. **10**, 950 (1998).
⁴ J.J. Neumeier and D.H. Goodwin, J. Appl. Phys. **85**, 5591 (1999).
⁵ J.J. Neumeier and J.L. Cohn, Phys. Rev. B **61**, 14319 (2000).
⁶ H. Aliaga, M.T. Causa, B. Alascio, H. Salva, M. Tovar, D. Vega, G. Polla, G. Leyva, and P. Konig, J. Magn. Magn. Mater. **226-230**, 791 (2001).
⁷ P.-G. de Gennes, Phys. Rev. **118**, 141 (1960).
⁸ L.-J. Zou, Q.-Q. Zheng, and H.Q. Lin, Phys. Rev. B **56**, 13669 (1997).
⁹ S. Yunoki, J. Hu, A. L. Malvezzi, A. Moreo, N. Furukawa, and E. Dagotto, Phys. Rev. Lett. **80**, 845 (1998).
¹⁰ D.P. Arovas and F. Guinea, Phys. Rev. B **58**, 9150 (1998).
¹¹ M. Yamanaka, W. Koshibae, and S. Maekawa, Phys. Rev. Lett. **81**, 5604 (1998).
¹² E.L. Nagaev, Phys. Rev. B **58**, 2415 (1998).
¹³ M.Yu. Kagan, D.I. Khomskii, and M.V. Mostovoy, Eur. Phys. J. B **12**, 217 (1999).
¹⁴ S. Yunoki and A. Moreo, Phys. Rev. B **58**, 6403 (1998).
¹⁵ E. Dagotto, S. Yunoki, A. L. Malvezzi, A. Moreo, J. Hu, S. Capponi, D. Poilblanc, and N. Furukawa, Phys. Rev. B **58**, 6414 (1998).
¹⁶ S.-Q. Shen and Z.D. Wang, Phys. Rev. B **58**, R8877 (1998).
¹⁷ H. Yi, and J. Yu, Phys. Rev. B **58**, 11123 (1998).
¹⁸ S.M. Dunaevsky and V.V. Deriglazov, Phys. Rev. B **67**, 014409 (2003).
¹⁹ M. Hennion, F. Moussa, J. Rodríguez-Carvajal, L. Pinsard, and A. Revcolevschi, Phys. Rev. B **56**, R497 (1997).
²⁰ M. Hennion, F. Moussa, G. Biotteau, J. Rodríguez-Carvajal, L. Pinsard, and A. Revcolevschi, Phys. Rev. Lett. **81**, 1957 (1998).
²¹ M. Hennion, F. Moussa, G. Biotteau, J. Rodríguez-Carvajal, L. Pinsard, and A. Revcolevschi, Phys. Rev. B **61**, 9513 (2000).
²² for a recent review, see K.H. Kim, M. Uehara, V. Kiryukhin, and S.-W. Cheong, preprint, cond-mat/0212113, and references therein.
²³ J.L. Cohn and J.J. Neumeier, Phys. Rev. B **66**, 100404(R)

- (2002).
- ²⁴ E. Granado, N. O. Moreno, H. Martinho, A. García, J. A. Sanjurjo, I. Torriani, C. Rettori, J. J. Neumeier, and S. B. Oseroff, *Phys. Rev. Lett.* **86**, 5385 (2001).
- ²⁵ M.M. Savosta, P. Novák, M. Marysko, Z. Jiráček, J. Hejtmánek, J. Englich, J. Kohout, C. Martin, and B. Raveau, *Phys. Rev. B* **62**, 9532 (2000).
- ²⁶ C.D. Ling, E. Granado, J.J. Neumeier, J.W. Lynn, and D.N. Argyriou, following paper.
- ²⁷ N.W. Ashcroft and J. Lekner, *Phys. Rev.* **145**, 83 (1966).
- ²⁸ An estimation of the difference between the average magnetization inside and outside the droplets (δM) may be obtained from the cross sections, as described in ref.²⁰. We obtain $\delta M = 6(3) \mu_B/\text{Mn}$ for $x = 0.02$ and $x = 0.09$. The large standard deviation is mostly due to the uncertainty in the cluster volume. For $x = 0.09$, we considered that the droplets are distributed in the $\sim 50\%$ volume fraction occupied by the G-AFM + FM mesoscopic domains (see text and Ref.²⁶). Thus, the actual differential cross sections for droplet scattering from such mesoscopic domains is twice the sample-average cross sections shown in Fig. 1(b). The fitting parameter N_V refers, by definition, to the cluster concentration inside the mesoscopic domains where the clusters are located.
- ²⁹ E. Granado, H. Martinho, M.S. Sercheli, P.G. Pagliuso, D.D. Jackson, M. Torelli, J. W. Lynn, C. Rettori, Z. Fisk, and S. B. Oseroff, *Phys. Rev. Lett.* **89**, 107204 (2002).
- ³⁰ Y.-R. Chen and P.B. Allen, *Phys. Rev. B* **64**, 064401 (2001).
- ³¹ T. Shibata, B. Bunker, J.F. Mitchell, and P. Schiffer, *Phys. Rev. Lett.* **88**, 207205 (2002).
- ³² P. N. Santhosh, J. Goldberger, P.M. Woodward, T. Vogt, W.P. Lee, and A.J. Epstein, *Phys. Rev. B* **62**, 14928 (2000).
- ³³ M. Pissas, G. Kallias, M. Hofmann, and D. M. Többens, *Phys. Rev. B* **65**, 064413 (2002).
- ³⁴ M. Pissas and G. Kallias, preprint, cond-mat/0205410.